Developing an Enhanced Computational Framework for Simulating Myocyte Membrane Mechanics: Catch-Bond Dynamics and Algorithmic Optimization

Shuxuan Wang *

Wuhan Britain-China School, Wuhan 430000, China

* Corresponding Author Email: shuxuanwang114@gmail.com

Abstract. The loading and mechanical deformation of myocytes provide important information about muscular deficits, particularly Duchenne Muscular Dystrophy (DMD). Although current computational models generally treat the interaction of the cell membranes and cytoskeletons as a slip bond, they do not accurately simulate the dynamic properties of catch bonds in a physiological setting. This paper describes an upgraded computational method for simulating the mechanical response of myocytes by implementing an upgraded two-state catch bond model that is capable of representing multiple dynamic velocity profiles when simulating cell responses to loading conditions. Additionally, a variance-preserving prefix-sum algorithm has been created to represent the non-homogeneous Poisson process in a more efficient manner. The development of this algorithm decreased the level of computational complexity from $O(n^2)$ to $O(n)$, thus enabling larger-scale simulations. As part of the validation process, the developed method was implemented on cells undergoing deformation through four biological states: normal (healthy cells), stiffened (abnormal), aged (senescent), and diseased (DMD), yielding results consistent with established theories of biomechanics and mechanobiology.

Keywords: Computational Biomechanics; Membrane Tethering; Catch-bond; Myocyte Mechanics; Algorithm Optimization.

1. Introduction

Chemical energy is converted to mechanical force by myocytes and these cells are considered highly specialized, as they provide both active contractions (contraction upon demand) and passive mechanical responses (contraction as a result of resistance to tension). The ability for myocytes to sense and respond to mechanical forces is dependent on the structural integrity of both their membranes and their cytoskeletons; therefore, both the membrane and cytoskeleton must be intact for a myocyte to correctly sense and respond to the mechanical forces acting upon it. Myocytes are affected by pathophysiological conditions (such as Duchenne Muscular Dystrophy (DMD)) and normal physiological aging, causing the mechanical properties of the myocytes (e.g., increased stiffness and decreased membrane stability) to be significantly impaired. Thus, the measurement of any change in the mechanical properties of myocytes will aid in understanding the mechanisms of disease states.

Experimental methodologies, such as atomic force microscopy (AFM), are useful for generating laboratory-based data as well as for revealing experimental limitations (due to lack of throughput and challenges isolating mechanical variables); however, they do not allow for the same degree of resolution of behavior in experimental conditions [4], which makes using computational modeling to build cell deformation (e.g., membrane tether extraction) models a possible alternative approach [5]. The majority of computational modeling techniques use relatively crude simplifications like treating receptor-ligand interactions as non-specific and having constant pulling velocities [6]; consequently, these systems are not well suited to describe the most biologically relevant characteristics, such as catch-bond behavior [7], where the bond lifetime increases with increasing force applied to the receptor-ligand system. Furthermore, computational modelling has not adequately modelled dynamic loading on cells in vivo.

This research proposes the development and validation of a new, more advanced computational model for simulating the mechanical behavior of myocytes in comparison to any currently available models for simulating the mechanical behavior of myocytes. This newly developed computational model is based on the underlying biophysical principles and includes the incorporation of a two-state catch-bond model that allows for adjustable rate of loading. In addition, to address issues related to calculating the time required to perform the stochastic bond breaking simulations, a prefix sum algorithm was developed that results in substantial improvement to the rate of performing these simulations. This model has been validated based on both simulated and measured data for myocyte mechanical behavior under normal, stiffened, aged and diseased environments.

2. Methodology

2.1. Cell Kinematics Model

Cell mechanics are represented using a three-parameter solid model, the Standard Linear Solid (SLS). This model consists of two components: a spring with modulus E_1 in series with a Kelvin-Voigt element (consisting of E_2 in parallel with a dashpot η) [8]. The relationship between stress and strain is defined as follows:

$$\sigma + \tau_\epsilon \frac{d\sigma}{dt} = E_R \left(\epsilon + \tau_\sigma \frac{d\epsilon}{dt}\right) \tag{1}$$

where $\tau_\epsilon = \eta/E_2,\ \tau_\sigma = \eta/(E_1 + E_2)$, and $E_R = E_1$. To calculate the total strain under arbitrary force history, a hereditary integral approach is implemented, approximated by discrete summation at each timestep dt:

$$\epsilon(t) = \int_0^t J(t-\zeta)\frac{d\sigma(\zeta)}{d\zeta}d\zeta \tag{2}$$

2.2. Catch-Bond Implementation

An important improvement of the model within this framework is the introduction of a catch bond instead of a slip bond, since it allows for modeling of mechanically enhanced adhesion. The catch bond is modeled using a two-state system with the bond alternating between a "slip" (weak) state and a "catch" (strong) [7]. The on and off rates from each of these states ($k_{10},\ k_{20}$), as well as the rate that each of these bonds transitions between states ($k_{12},\ k_{21}$) are all dependent upon the force applied, and are determined by the characteristic forces of each bond ($F_{10},\ F_{20},\ F_{12},\ F_{21}$).

$$\begin{aligned} k_{10}(F) &= k_{10}^0 \exp\left(\frac{F}{F_{10}}\right), k_{20}(F) = k_{20}^0 \exp\left(\frac{F}{F_{20}}\right) \\ k_{12}(F) &= k_{12}^0 \exp\left(\frac{F}{F_{12}}\right), k_{21}(F) = k_{21}^0 \exp\left(-\frac{F}{F_{21}}\right) \end{aligned} \tag{3}$$

This allows the effective off-rate $k_{off}(F)$ to vary dynamically with the applied load, capturing the counterintuitive strengthening of bonds under specific force ranges.

2.3. Algorithmic Optimization: The Prefix Sum Approach

Simulating the stochastic breaking of bonds with time-varying rates requires solving the non-homogeneous Poisson process. The probability of breaking P_{off} at time t is:

$$P_{off} = 1 - \exp\left(-\int_0^t k_{off}(F(\tau))d\tau\right) \tag{4}$$

In a naive implementation, calculating the integral $\int_0^t$ at every timestep t requires scanning all previous history, leading to a computational complexity of $O(n^2)$, where n is the number of timesteps. This becomes prohibitively slow for long-duration simulations.

To resolve this, a prefix-sum optimization was implemented. A running cumulative sum of the hazard function is maintained:

$$\text{prefix\_sum}\,[t] = \text{prefix\_sum}\,[t-1] + k_{off}(F(t))\Delta t \tag{5}$$

This reduces the complexity of calculating the breaking probability to $O(1)$ per timestep, and the total simulation complexity to $O(n)$. This optimization is critical for enabling high-resolution simulations with small dt.

2.4. Dynamic Pulling Speed Support

The model was extended to support dynamic pulling speeds $U_p(t)$ via a customizable function interface. Unlike constant-speed models, the total pulling length $L(t)$ and force change $\Delta F(t)$ are updated iteratively:

$$L(t) = L(t-1) + U_p(t)\Delta t \tag{6}$$

This feature allows researchers to simulate complex scenarios, such as the variable deceleration phases observed in leukocyte rolling [9], which were previously infeasible.

3. Validation and Results

To validate the computational framework rigorously, a series of baseline tests were created. The mechanical responses demonstrated by the myocytes were compared across four distinct physiological states. The parameters for the normal state were determined based on previous studies [10-13]. The parameters for stiffened, aged, and diseased states have been adapted to reflect the biomechanical trends demonstrated in the literature by other researchers [14, 15]. All parameter sets are documented in Table 1.

3.1. Simulation Setup

To compare the results with other research studies, the pulling speed and the probe stiffness were set at standard levels (2 μm/s and 100 pN/μm, respectively), and the time step was set at one second. A main objective of this work was to assess if this model can recreate the abnormal deformation patterns that are characteristic of diseases.

Table 1. Key Parameters for Validation Simulations

Cell Condition	$k_c(pN/\mu m)$	$k_i(pN/\mu m)$	$F_0(pN)$	$k_{cyt}(s^{-1})$
Normal	15000	45	35	1.0
Stiffened	30000	80	50	0.5
Aged	12000	25	20	2.0
Diseased	18000	15	10	5.0

3.2. Cell Surface Deformation and Velocity

In Figure 1, the time-dependent changes in the deformation of cell surfaces are depicted. Diseased cells (red) exhibit the earliest and largest deformation compared to other cell types, indicating lower resistance to applied loads. Stiffened cells (which simulate fibrotic tissue) were the most resistant to the initial deformation. The higher level of deformability in the red line corresponds with DMD's loss of cytoskeletal stability [2].

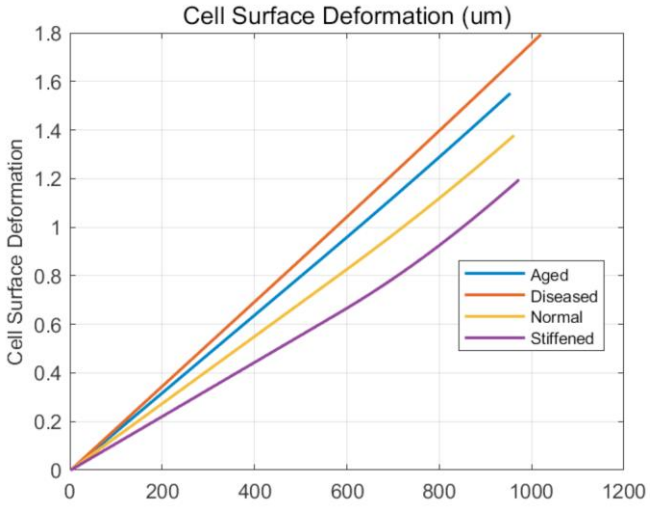

Figure 1. Validation of surface deformation across four cell states.

The analysis of cell surface velocity (Figure 2) indicates a two-phase behavior, which is an initial phase that reflects steady-state velocity followed by a second phase of acceleration. Stiff cells move faster than other types of cells during Phase II of the Velocity Profile. This shows that once deformation has surpassed the mechanical threshold, a series of rapid events that result in structural failure occurs. The point at which the Velocity Profile curve transitions from a steady state to an increasing slope is representative of the extraction phase of the membrane tethers. In a physiological context, this transition represents the disconnecting of the lipid bilayer from the cytoskeleton. While stiffened cells (represented by the purple line) have a higher degree of resistance to deformation in the first phase (in terms of velocity), they exhibit an accelerated velocity profile during the second phase. The findings suggest that stiffness results in increased structural strength and fiber matrix stiffness, which may support stiffness under static load, but at the same time causes failure to occur under dynamic load when the threshold is reached. Stiffened cells are considered to retain energy that is accumulated throughout the entire deformation process, which can be released in a short time period upon rupturing of the bond, thus providing a possible explanation for how fibrotic tissues are likely to tear rapidly under high-load conditions.

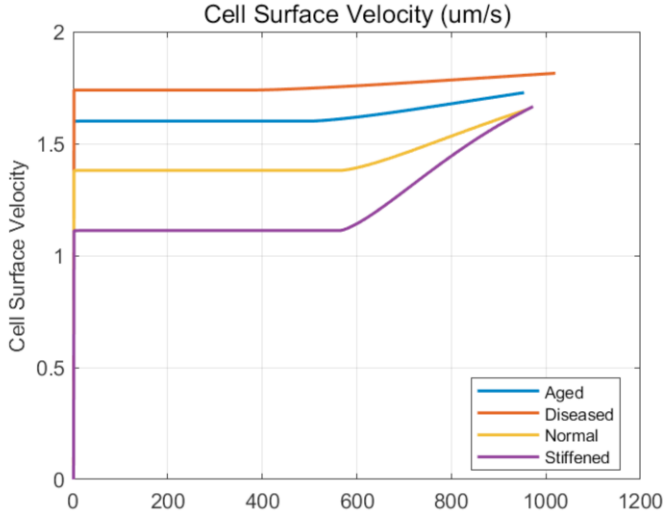

Figure 2. Comparison of cell surface velocity.

3.3. Membrane Tether Dynamics

The nonlinear dynamics of tether pulling were accurately captured by the model as presented in Figures 3 and 4. Tether assembly occurred throughout the time period from t =400s to t =600s, for all conditions.

Figure 3 reveals a surprising insight: despite initially resisting extraction, stiffened cells generate the longest-lasting tethers post-extraction. The following provides rationale for this insight: The ability for Stiffened cells to produce greater than average tether lengths is related to energy conservation and catch-bond behavior. A compliant cell type (diseased or aged) has a greater amount of viscous elasticity present in its cellular body and, therefore, has a high degree of viscoelastic deformation, which allows it to use a greater portion of its extracted work on deformation prior to the formation of tethers. However, since the Stiffened cell is very stiff, it behaves as a solid anchor and therefore dissipates very little of the energy generated by pulling on it. Hence, after the tether attachment and its associated catch bonds were broken, a significant and rapid extraction of the remaining membrane of the cell occurred due to the catch bonds' maintenance of the high tension associated with their elastic stretching under the pulling process. Thus, Figure 4 supports this view, showing that Stiffened cells exhibit the highest velocity at the end of tether formation.

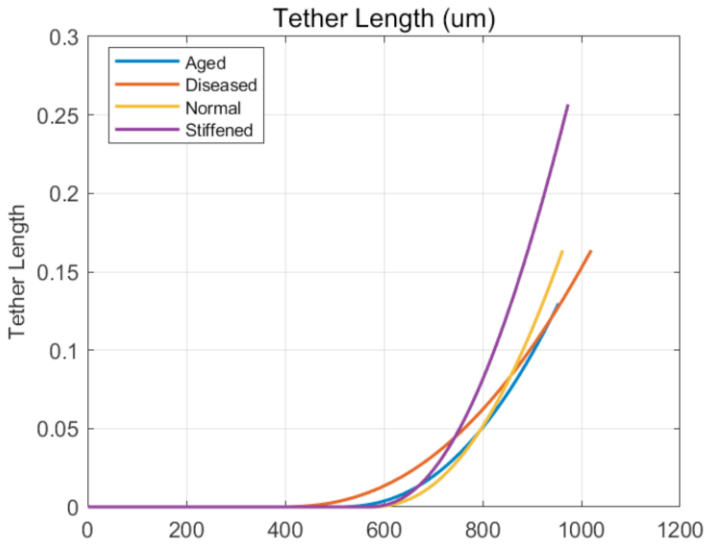

Figure 3. Simulation of membrane tether growth.
Stiffened cells (purple) produce the longest tethers post-extraction, despite their initial resistance.

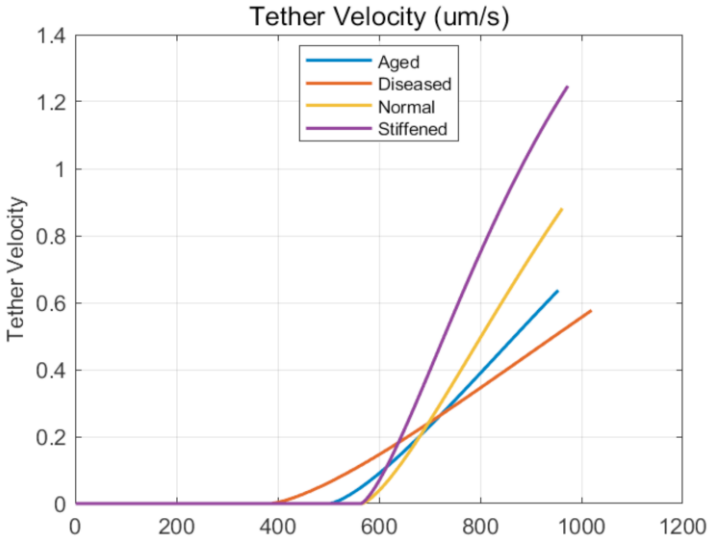

Figure 4. Tether extraction velocity.

The model characterizes a range of kinetic response variability, whereby diseased cells demonstrate early and gradual extraction of kinetic energy while cells that are stiffened show a late and rapid extraction of energy as compared to diseased cells. The findings support the computational framework proposed within the present study as a robust framework to distinguish subtle mechanical

strategies (e.g., normal cells exhibit "compliance-mediated" protection as opposed to diseased cells exhibiting "stiffness-induced" brittleness).

4. Discussion

This research has developed a computational model that simulates cell mechanics at a higher resolution than what was previously available by combining the catch-bond dynamics with an efficient prefix-sum algorithm and tested against known biological data for both its effectiveness and the resulting output.

Computationally this model closely matches the expected output for cells that have previously been identified in the literature as having a high risk of instability (DMD). Moreover, the diseased cell's ability to respond to stress early in the model, when compared to healthy muscle tissue, demonstrated membrane tethering is an early indicator of muscle membrane failure in humans [2]. The response of the stiffened cells exhibited a similar mechanical behavior to the mechanical behavior exhibited by fibrotic tissue; initial stiffness that produced a large yield point at time zero resulted in catastrophic cell behavior.

The major benefit of the current framework is its extensibility. By accommodating dynamic variations in the pulling speed for model systems, it can simulate and recreate conditions seen during the actual physiological process, such as the variation in the pull of muscle contractions at any given time. While this framework can be considered a major advantage to researchers, it does have some limitations. The current parameters used to represent diseased states were derived by modifying those of the general knowledge of healthy states because there are no complete sets of experimental data available. Future efforts will work on conducting a comprehensive sensitivity analysis of the relationship between catch-bond parameters ($F_{10},\ F_{20}$) and the global deformation profile as defined through the experimental outcomes.

5. Conclusion

This study reports on the advances in the development and validation of a novel enhanced computational framework for simulating deformation of myocytes due to load-bearing forces. The incorporation of catch bonds, along with the $O(n)$ optimization algorithm, enables detailed modeling of myocyte dynamic behavior, overcoming the limitations of previous slip-bond-only models. Baseline simulations demonstrate that this new simulation methodology may allow for future in-silico research on muscular dystrophy, increases in heart rate, and drug screening.

References

[1] Head S I, Williams D A, Stephenson D G. Abnormalities in structure and function of limb skeletal muscle fibres of dystrophic mdx mice. Proceedings of the Royal Society of London. Series B: Biological Sciences, 1992, 248(1322): 163-169.

[2] Remington J, Wang X, Hou Y, et al. Injection of recombinant human type VII collagen corrects the disease phenotype in a murine model of dystrophic epidermolysis bullosa. Molecular Therapy, 2009, 17(1): 26-33.

[3] Lacraz G, Rouleau A J, Couture V, et al. Increased stiffness in aged skeletal muscle impairs muscle progenitor cell proliferative activity. PloS one, 2015, 10(8): e0136217.

[4] Hochmuth R M. Micropipette aspiration of living cells. Journal of biomechanics, 2000, 33(1): 15-22.

[5] Alvarez D, Sapia J, Vanni S. Computational modeling of membrane trafficking processes: from large molecular assemblies to chemical specificity. Current Opinion in Cell Biology, 2023, 83: 102205.

[6] Shao J Y, Yu Y, Oswald S J. From Surface Protrusion to Tether Extraction: A Mechanistic Model. ACS Biomaterials Science & Engineering, 2017, 3(11): 3036-3042.

[7] Sokurenko E V, Vogel V, Thomas W E. Catch-bond mechanism of force-enhanced adhesion: counterintuitive, elusive, but… widespread?. Cell host & microbe, 2008, 4(4): 314-323.

[8] Achenbach J D, Chao C C. A three-parameter viscoelastic model particularly suited for dynamic problems. Journal of the Mechanics and Physics of Solids, 1962, 10(3): 245-252.

[9] McEver R P, Ramachandran V, Williams M, et al. Cellular and molecular features that stabilize rolling on selectins under flow. In Proceedings of the Second Joint 24th Annual Conference and the Annual Fall Meeting of the Biomedical Engineering Society, 2002: 331-332.

[10] Collinsworth A M, Zhang S, Kraus W E, et al. Apparent elastic modulus and hysteresis of skeletal muscle cells throughout differentiation. American Journal of Physiology-Cell Physiology, 2002, 283(4): C1219-C1227.

[11] Dai J, Sheetz M P. Mechanical properties of neuronal growth cone membranes studied by tether formation with laser optical tweezers. Biophysical journal, 1995, 68(3): 988-996.

[12] Lieber R L, Shah S, Fridén J. Cytoskeletal disruption after eccentric contraction-induced muscle injury. Clinical Orthopaedics and Related Research®, 2002, 403: S90-S99.

[13] Evans E A, Calderwood D A. Forces and bond dynamics in cell adhesion. Science, 2007, 316(5828): 1148-1153.

[14] Wells R G. The role of matrix stiffness in regulating cell behavior. Hepatology, 2008, 47(4): 1394-1400.

[15] Harris A R, Peter L, Bellis J, et al. Characterizing the mechanics of cultured cell monolayers. Proceedings of the National Academy of Sciences, 2012, 109(41): 16449-16454.